Acoustic input impedance of the avian inner ear measured in ostrich (Struthio camelus)

Acoustic input impedance of the avian inner ear measured in ostrich (*Struthio camelus*)

Pieter G.G. Muyshondt[a,1], Peter Aerts[b] and Joris J.J. Dirckx[a]

[a] *University of Antwerp, Laboratory of Biophysics and Biomedical Physics, Groenenborgerlaan 171, 2020 Antwerp, Belgium*
[b] *University of Antwerp, Functional Morphology, Universiteitsplein 1, 2610 Antwerp, Belgium*

[1] *Email address:* pieter.muyshondt@uantwerpen.be

Abstract

In both mammals and birds, the mechanical behavior of the middle ear structures is affected by the mechanical impedance of the inner ear. In this study, the aim was to quantify the acoustic impedance of the avian inner ear in the ostrich, which allows us to determine the effect on columellar vibrations and middle ear power flow in future studies. To determine the inner ear impedance, vibrations of the columella were measured for both the quasi-static and acoustic stimulus frequencies. In the frequency range of 0.3-4 kHz, we used electromagnetic stimulation of the ossicle and a laser Doppler vibrometer to measure the vibration response. At low frequencies, harmonic displacements were imposed on the columella using piezo stimulation and the resulting force response was measured with a force sensor. From these measurement data, the acoustic impedance of the inner ear could be determined. A simple RLC model in series of the impedance measurements resulted in a stiffness reactance of K_{IE} = $0.20 \cdot 10^{12}$ Pa/m³, an inertial impedance of M_{IE} = $0.652 \cdot 10^{6}$ Pa s²/m³, and a resistance of R_{IE} = $1.57 \cdot 10^{9}$ Pa s/m. We found that values of the inner ear impedance in the ostrich are one to two orders in magnitude smaller than what is found in mammal ears.

Keywords

Avian ear; acoustic impedance; laser Doppler vibrometry; electromagnetic stimulation; piezo stimulation.

Highlights

- The acoustic input impedance of the inner ear was measured in ostrich
- Magnetically induced columellar vibrations were measured with LDV from 0.3 to 4 kHz
- Low-frequency vibrations were measured using piezo stimulation and a force sensor
- The stiffness, resistance and inertia of the inner ear impedance were determined

Abbreviations

C	columella
CT	computed tomography
FP	footplate
IE	inner ear
LDV	laser Doppler vibrometry
ME	middle ear
OW	oval window
RW	round window
SxL/R	left/right ear of specimen x
TM	tympanic membrane

1. Introduction

To date, there are two conflicting theories regarding the motions of the columella in the bird middle ear (ME): the first theory proposes that the ossicle performs side-to-side or rocking movements under stimulation of the tympanic

membrane (TM) (Gaudin, 1968), while the other theory proposes piston-like motions (Norberg, 1978). The nature of this motion is important since it influences the lever function of the ossicle that contributes to the impedance matching function of the ME.

Studies in human (e.g. Hato *et al*., 2003) have shown that the inner ear (IE) influences motions of the stapes. The predominant piston-like motions of the stapedial footplate (FP) are converted into rocking motions to some extent at higher stimulus frequencies, which is partially due to the presence of the IE fluid behind the oval window (OW). Also in reptiles and birds, the impedance of the IE is assumed to affect columellar FP vibrations (Gummer *et al*., 1989b) and the behavior of the ME in general (Manley, 1972). To study the motions of the ossicles and the corresponding influence of the IE, measurement data are needed of the acoustic input impedance of the IE.

In humans and other mammals, the acoustic input impedance of the IE has been estimated and measured in several ways (e.g. Zwislocki, 1965; Lynch *et al*., 1982; Kringlebotn, 1988; Merchant *et al*., 1996; Puria *et al*., 1997; Aibara *et al*., 2001). The IE impedance of birds is presumably different from mammals because of differences in IE size and structure. The auditory portion of the IE in birds is not coiled but straight as opposed to the cochlea in mammals. Also, the architecture of the basilar membrane inside the cochlear duct is different, and the ratios of the surfaces of the round window (RW) and OW are dissimilar, which is assumed to contribute to the IE impedance as well (Merchant *et al*., 1996).

In this study, the acoustic input impedance of the IE is determined in the ostrich (*Struthio camelus*). In the acoustic frequency range, the IE impedance is determined with laser Doppler vibrometry (LDV) and digital stroboscopic holography. As stimulation source, an electromagnetic induction solenoid and a magnet attached to the ossicle are used. In the quasi-static regime, a piezo transducer and force sensor are utilized to measure the IE impedance.

2. Methods

2.1 Acoustic impedance

The method used to measure the acoustic impedance of the IE (Z_{IE}) is similar to the approach followed in Merchant *et al*. (1996). With this approach, the acoustic impedance of the columella and the IE combined (Z_{CIE}) is calculated from measurements of the columellar velocity v_C with intact IE, in response to stimulation forces measured at the distal end of the columella (F_C). The acoustic impedance is defined as

$$Z = \frac{p_C}{U_C} = \frac{F_C}{v_C \cdot A_{FP}^2}, \tag{1}$$

in which p_C is the pressure acting on the columellar FP in the OW, U_C the volume velocity of the FP and A_{FP} the total surface area of motion of the FP. This area includes the medial surface area of the bony columellar FP, but also a portion of the annular ligament that surrounds the FP in the OW and vibrates along with the FP. The measurement procedure is repeated with an opened IE to determine the acoustic impedance of the columella Z_C, which incorporates the impedance of the bony ossicle and the annular ligament. The acoustic impedance of the IE (Z_{IE}) is then calculated by subtracting Z_C from Z_{CIE}.

With the followed approach, several assumptions are made: (1) motions of the columella are piston-like in the current setup, (2) forces (resp. velocities) measured on the distal end of the columella are equal to the forces (resp. velocities) acting on FP in the OW, (3) velocities measured on the columella are in the linear response regime for the applied stimulus levels, and (4) the passive properties of the dead IE were not altered after the sample preparations.

In the human temporal bone study by Merchant *et al*. (1996) it was possible to stimulate the stapes acoustically and shield the RW from this stimulation. In the ostrich this is not possible as the RW is very large and is located in close vicinity of the FP, so an acoustic stimulus would reach both structures. We therefore used different stimulation techniques which are explained in detail in the following sections.

2.2 Sample preparation

Ostriches were chosen as model species because they are the largest existing avian species, so the ear is large enough to perform the needed manipulations. The heads of 8 ostriches, with ages between 1.5 and 5 years, were obtained from an ostrich farm. The samples were frozen one day after death and thawed right before measurement. Studies in human (Ravicz *et al*., 2000) have shown that it is possible for air to penetrate the IE during the freezing and thawing process, which may alter the IE impedance. Therefore, each sample was checked for the presence of air

bubbles behind the RW membrane before measurement. Subsequently, the ear canal, the TM and the cartilaginous extracolumella, which connects the TM to the columella, were removed. Also, half of the columellar shaft was cut from the distal side of the ossicle. To obtain optical access of the columella and the FP, some of the surrounding bone and soft tissues were removed without breaking up the IE structures. Vibration measurements were performed after each of the following manipulations. First, the IE was left intact. Then, the RW membrane was perforated with a needle. Next, the IE was thoroughly drained with a suction tip through the perforation in the RW. Finally, the medial walls of the IE were drilled to remove the remaining IE fluid that was left on the medial surface of the columellar FP.

2.3 Experiments in the acoustic regime

2.3.1 Laser Doppler vibrometry

To induce columellar vibrations in the acousic frequency range, magnetic stimulation of the ossicle was used, which is a technique that was previously applied to study ossicular fixation in human temporal bones (e.g. Peacock *et al*., 2013). A schematic overview of the experimental setup is shown in Fig. 1 (a). A small gold-coated neodymium magnet with a mass of 3 mg was fixated with superglue (Loctite, Super Glue Precision, Düsseldorf, Germany) on the tip of the remaining distal part of the columella. Then, a miniature copper induction solenoid was placed over the magnet using a translation stage to adjust the position of the coil in three directions. The force that the induction coil exerts on the electromagnet was calibrated using a scale with a precision of 1 µN. During the measurements, alternating sinusoidal currents were run through the coil to stimulate the magnet using stepwise frequencies between 0.25 and 4 kHz, with 16 lines per octave. At the same time, the induced vibration response of the columella was measured with a single-point one-dimensional laser Doppler vibrometer (Polytec, OFV-534 sensor head and OFV-5000 controller, Waldbronn, Germany) mounted on a surgical microscope (Carl Zeiss, OPMI Sensera/S7, Jena, Germany). Vibrations of the columella were measured on the lateral side of the electromagnet in a direction parallel to the columellar shaft and the induced magnetic field. To increase the reflection of the laser beam on the specimen, a small piece of reflective tape was placed on top of the magnet. To control and analyze the stimulation and response signals, a program was developed in Matlab (Mathworks, Natick, MA, USA) that interacts with a data acquisition device (National Instruments, USB-6251 BNC, Austin, TX, USA) to generate the electromagnetic stimulus and to measure the stimulation and response signals simultaneously. The data acquisition card was set at a sample rate of 48 kHz. Each signal was extended with 0.1 s to eliminate transient effects in the response. Subsequently, the amplitude of both signals and the phase difference between the two signals was determined from the Fourier transform of the waveforms at the applied stimulus frequencies. Electronic phase delays in the experimental setup were accounted for.

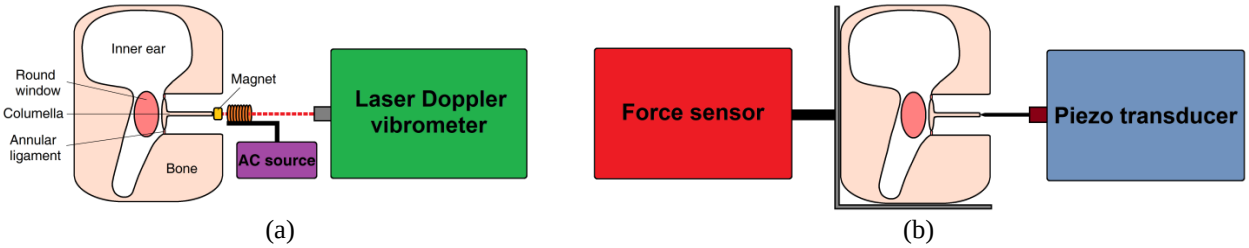

Figure 1. Schematic overview of the experimental setups. (a) Setup for the measurements in the acoustic regime. A magnet is placed on the distal end of the columella and stimulated by a miniature induction coil through which an alternating current is sent. A laser Doppler vibrometer measures the induced columella vibration velocities on top of the magnet. (b) A piezo transducer stimulates the columella on the distal end with a needle at controlled displacement amplitude. The induced forces on the specimen are measured with a force sensor.

2.3.2 Digital stroboscopic holography

In order to determine the IE impedance with the LDV setup and the electromagnetic stimulation, the assumption was made that columellar displacements are piston-like. To verify this assumption, the full-field out-of-plane displacements of the columellar FP were measured with digital stroboscopic holography. Very short laser pulses (3 ns) were synchronized with the phase of the vibrating object, so that full-field displacements of the object's surface

could be calculated at the chosen phase. By cycling these pulses stepwise through the vibration period, the entire time-dependent motion the surface was obtained. More details on the technique can be found in Cheng *et al*. (2010, 2013), Khaleghi *et al*. (2013) and De Greef *et al*. (2014). In the current holography setup, the columella is stimulated electromagnetically in the same way as in the LDV setup, but the displacement response is measured from the medial side of the columellar FP instead of from the lateral side. To expose the FP, the IE needed to be removed for the measurements. To enhance reflectivity of the sample, the medial side of the FP was coated with white make-up liquid (Kryolan, Kryolan Aquacolor Soft Cream - White Wet Make-up, Product Code 01129/00, Berlin, Germany).

2.4 Experiments in the quasi-static regime

To study the quasi-static properties of the acoustic IE impedance, a piezo transducer (Physik Instrumente, P-864.10, Karlsruhe, Germany) was used to induce displacements of columella. A scheme of the measurement setup is shown in Fig. 1 (b). The piezo transducer contains an embedded strain gauge that has an active feedback loop, so the displacements could be controlled to a precision better than 50 nm. The frequency-dependence of the piezo system was calibrated by measuring its actual displacement amplitude with LDV. During measurement, the needle of the piezo transducer was positioned on the remaining distal end of the columella, in a direction parallel to the columellar shaft. The position of the needle was further adjusted under the microscope such that columellar displacements were purely piston-like. At the same time, the forces provoked by the displacements were measured with a force sensor (LCM Systems Ltd, UF1 Force Sensor, Newport, Isle of Wight, UK). The ear specimen was placed and glued on a holder connected to the force sensor, after dissecting the ear from the head. The sensor contains a load cell that can detect forces as small as 1 mN. The force sensor was integrated in the experimental setup using custom-made electronics. Forces that the specimen exerts on the force sensor were measured parallel to the displacement stimulus of the piezo needle. To control and analyze the displacement stimulus and the force response, the same software was used as for the acoustic frequency measurements. The resulting columellar velocity v_C was determined by $v_C = i\omega x_C$, with i the imaginary unit, ω the angular frequency and x_C the measured columellar displacement.

2.5 Footplate surface area

According to Eq. (1), the acoustic impedance of the IE depends on the square of the total surface area of the FP. To determine this area accurately, microphotographs were made of the medial surface of the FP with a high-resolution digital CCD camera (Foculus, F0442B /SC IEEE1394, Aegis Electronic Group, Gilbert, AZ, USA) after vibration measurement of the sample. The camera has a resolution of 1392 x 1040 square pixels and the images were calibrated at 2.2 µm per pixel. Before the images were made, the columella was removed from the sample and positioned in front of the camera by means of a horizontal and vertical translation stage. In the analysis of the images, the surface of the bony columella was extracted using a threshold filter. The remaining surrounding tissue of the annular ligament was not incorporated in this surface.

Since the annular ligament partially moves along with the FP during vibration, it contributes to the total volume displacement in the OW and hence the impedance of the IE. To quantify the volume displacement that is attributed to the annular ligament, full-field holography measurements were performed on the medial side of the FP for a single sample, as described in section 2.3.2. From the resulting full-field displacement map, the total volume displacement was determined as a function of the volume displacement that only belongs to the bony FP.

3. Results

3.1 Footplate surface area

Table 1 shows the surface areas of the columellar FPs measured with microphotography. As can be deduced from the table, not each specimen was measured on both sides of the head. The mean surface area of all samples was equal to 3.03 mm² with a standard deviation of 0.41 mm². Holography measurements performed on the FP revealed that the total surface of motion in the OW equals 165% of the area of bony FP surface (data not shown), when averaged over multiple stimulus frequencies.

Table 1. Surface area of the medial side of the columellar FPs. The left column contains the specimen number, the second column shows the surface area on the left side of the head of the specimen, and the third column shows the FP area on the right side of the head.

Specimen number	Left side (mm²)	Right side (mm²)
1	3.19	3.17
2	3.05	2.93
3	2.41	2.53
4	3.03	2.86
5		2.69
6	3.36	3.42
7	3.54	3.74
8		2.50

3.2 Experiments in the acoustic regime

3.2.1 Laser Doppler vibrometry

LDV measurements were made for stimulus frequencies between 0.25 and 4 kHz, with 16 lines per octave. The maximum frequency of 4 kHz was chosen in relation to the upper frequency limit of hearing in the emu (*Dromaius novaehollandiae*), which is a species closely related to the ostrich which we found in literature (Manley *et al*., 1997). The amplitude of the electromagnetic force stimulus was equal to 0.1 mN, resulting in FP displacement amplitudes between 5 nm and 5 µm. Figure 2 shows the acoustic impedance calculated from the LDV measurements of (a) intact IE, (b) opened IE and (c) the difference of the two conditions that represents the impedance of the IE itself. Results from intermediate steps in the manipulation of the specimens are not shown.

When comparing the impedance results of the intact and opened condition from Fig. 2 (a), it is seen that impedance magnitudes are consistently higher when the IE is still intact. Only at the lowest and highest frequencies shown, magnitude values are similar. Peak magnitudes become sharper when the IE is opened, while being shifted to higher stimulus frequencies. This is also reflected in the phase response, in which the transition from -0.25 to +0.25 periods is much more sudden in the opened condition, although being postponed to higher frequencies. In the higher frequency range, the magnitude and phase both decrease for certain specimens with intact IE, but not with opened IE. Also, the variability in the measurements with intact IE is larger. For the impedance of the IE itself, we observe from Fig. 2 (c) that the magnitude and phase are similar to what is found for the intact condition in the middle frequency range. For lower and higher frequencies, the IE impedance deviates from the impedance with intact IE.

3.2.2 Digital stroboscopic holography

Holography measurements were performed for frequencies between 0.05 and 12.8 kHz, with 2 lines per octave. The chosen amplitudes of the stimulation force varied between 0.014 and 0.217 mN. Figure 3 shows the experimental results of the full-field FP displacement in the right FP of specimen 5 with opened IE, for the example frequencies of 0.1, 0.4, 0.8 and 1.9 kHz. Displacement magnitudes are normalized to the induced pressure of the electromagnetic stimulus, which was calculated from the force exerted on the magnet divided by the total area of motion in the OW.

At 0.1 kHz, the FP displacement magnitude contains two local maxima that have a relative phase difference of half a period, which shows that rocking motions are present in the vibrations of the columella in the current setup. This type of displacement pattern was seen for all measured frequencies between 0.05 and 0.3 kHz. Above 0.3 kHz, the displacement pattern altered, as shown in Fig. 3 for 0.4 kHz. At this frequency, the full-field displacement magnitude and phase are largely uniform, which is also the case for higher stimulus frequencies such as 0.8 and 1.9 kHz. This indicates that displacements at frequencies above 0.3 kHz are mostly piston-like. Because the motions are not piston-like below 0.3 kHz, we only present impedance data in the range of 0.3-4 kHz.

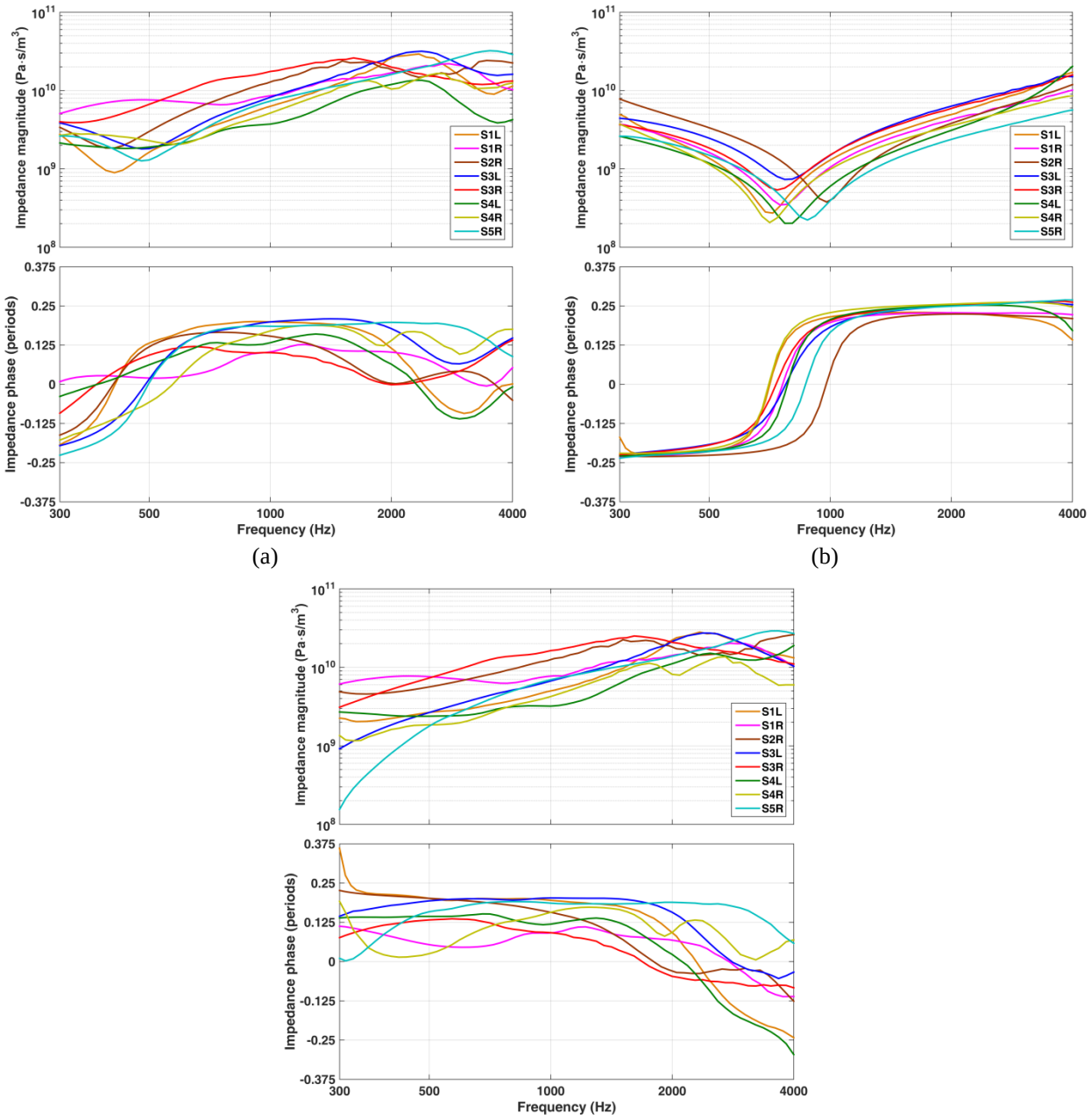

Figure 2. (a) Acoustic impedance magnitude (top) and phase (bottom) as a function of frequency, measured with (a) intact IE, (b) opened IE and (c) the difference between the two conditions for all measured ears.

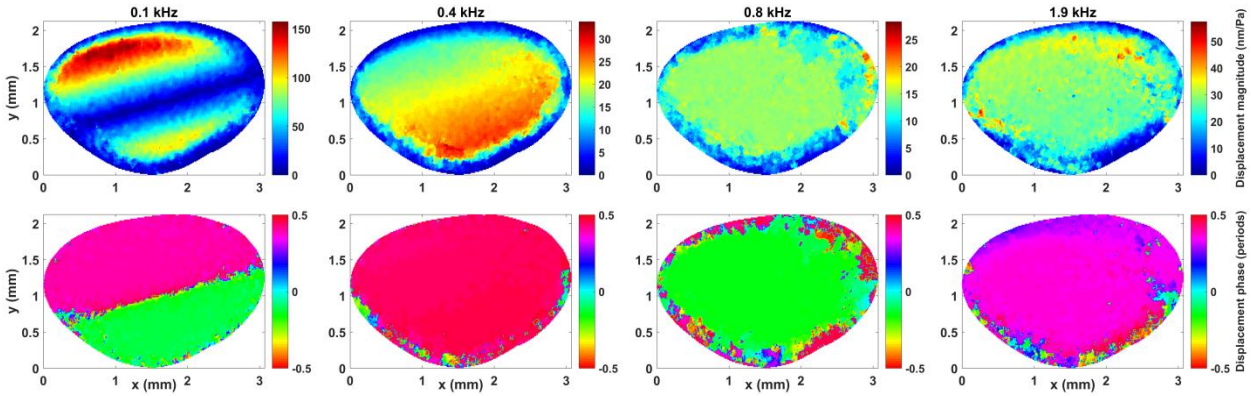

Figure 3. Full-field displacement response of the FP in the right ear of specimen 5 with IE opened, at stimulus frequencies of 0.1, 0.4, 0.8 and 1.9 kHz. The displacement magnitude (top) is normalized to incident pressure and for the displacement phase (bottom) the reference phase was chosen arbitrary.

3.3 Experiments in the quasi-static regime

Measurements of columella vibrations in the quasi-static regime using the piezo and force transducer were performed for frequencies from 1 to 20 Hz, with 1 line per octave. The amplitude of the displacement stimulus imposed by the piezo transducer was chosen equal to 50 µm. Figure 4 shows the magnitude of the acoustic impedance resulting from the displacement and force measurements, both with (a) intact IE, (b) opened IE and (c) the difference of both conditions that represents the impedance of the IE itself. Results of intermediate steps in the manipulation of the specimen are again not shown. The phase difference between the displacement stimulus and force response was measured at 1 Hz and found to be zero. For increasing frequency, the results of the phase measurements deteriorated due to experimental constraints and are therefore not presented.

In Fig. 4 (a) it is seen that the acoustic impedance in sample 6 is a bit larger than in sample 7. On the other hand, we observe that changes in the acoustic impedance after removal of the IE are almost negligible for each of the measured samples. This is also apparent from the IE impedance in Fig. 4 (b), in which impedances magnitudes are almost 2 orders smaller than in Fig. 4 (a).

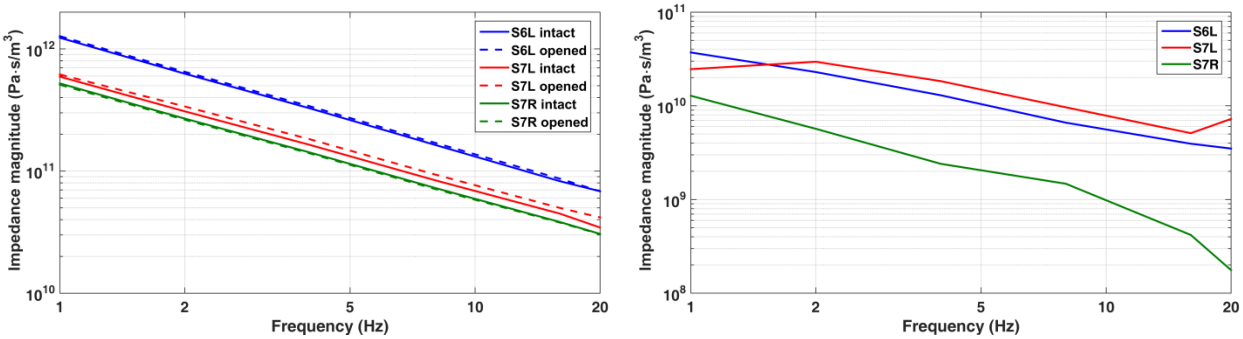

(a) (b)

Figure 4. Acoustic impedance magnitude as a function of frequency for (a) intact IE (solid lines), opened IE (dashed lines) and (b) IE impedance. Measurements were performed on the left ear of specimen 6 and on both ears of specimen 7.

3.4 Acoustic impedance analysis

The mean of the acoustic impedance measurements is shown in Fig. 5 (a). Due to the rocking motions found with holography, we could not determine the impedance in the frequency range between 0.02 and 0.3 kHz. The mean experimental impedance Z_{exp} was fitted for both intact IE and opened IE by using a simple RLC model in series Z_{mod} as in Merchant *et al.* (1996). In this model, the impedance is described by three components, namely the stiffness reactance K that is dominant in the low-frequency range, the inertial impedance M that is dominant in the high-frequency range, and the resistance R that dominates the impedance near the resonance frequency. In theory, K can

be determined from the low-frequency response by $K = \omega\ \mathrm{Im}(Z)$, with ω a low-valued angular frequency and Z the impedance measured at that frequency. M can be found through $M = K/\omega^2$, with ω the resonance frequency in which the impedance phase becomes zero. R can be calculated from M at the resonance frequency via $R = \omega M/Q$, with Q the so-called Q-factor that is defined as the ratio of the resonance frequency to the half-power bandwidth. To obtain the best fit, the least-squares method was used in which objective function χ^2 defined as

$$\chi^2(K) = \sum_i \left(\log\left|Z_{\mathrm{mod}}(\omega_i, K)\right| - \log\left|Z_{\mathrm{exp}}(\omega_i)\right|\right)^2 + \left(\angle Z_{\mathrm{mod}}(\omega_i, K) - \angle Z_{\mathrm{exp}}(\omega_i)\right)^2, \quad (2)$$

was minimized with respect to K. In this equation, $|Z|$ is the impedance magnitude, $\angle Z$ the unwrapped impedance phase and ω_i the stimulus frequencies from the measurements over which is summed in Eq. (2). The components M and R in the impedance model depend on K as defined in the current section. The weight given to each term in the sum of Eq. (2) is proportional to the number of measurements performed at the corresponding frequency.

The components of the impedance were found to be $K_{\mathrm{CIE}} = 7.25{\cdot}10^{12}$ Pa/m³, $M_{\mathrm{CIE}} = 0.952{\cdot}10^{6}$ Pa s²/m³ and $R_{\mathrm{CIE}} = 2.02{\cdot}10^{9}$ Pa s/m³ for intact IE and $K_{\mathrm{C}} = 7.05{\cdot}10^{12}$ Pa/m³, $M_{\mathrm{C}} = 0.300{\cdot}10^{6}$ Pa s²/m³ and $R_{\mathrm{C}} = 0.54{\cdot}10^{9}$ Pa s/m³ for opened IE. For each component, the difference of intact and opened IE was calculated yielding $K_{\mathrm{IE}} = 0.20{\cdot}10^{12}$ Pa/m³, $M_{\mathrm{IE}} = 0.652{\cdot}10^{6}$ Pa s²/m³ and $R_{\mathrm{IE}} = 1.57{\cdot}10^{9}$ Pa s/m³. These components represent the impedance of the IE itself, for which the corresponding RLC model is shown in Fig. 5 (b).

In Fig. 5 (a) we observe that the magnitudes of both models slightly overestimate the low-frequency measurements, while underestimating the high-frequency results. We also observe that the impedances with intact IE and opened IE strongly overlap in the low-frequency range, which is the case for both experiment and model. Between 0.3 and 1 kHz, the resonance peaks are nicely reflected in the models. For frequencies above 2 kHz, the sudden drop in the IE impedance of the intact condition cannot be reproduced by the model. The same is found for the impedance phase, in which the model fails to describe the intact IE for frequencies above 1 kHz. For opened IE the phase is predicted well by our model. For the IE impedance itself, shown in Fig. 5 (b), the model describes the magnitudes well for low and middle frequencies, although it must be highlighted that standard deviations are large in the low-frequency range. For the highest frequencies above 1 kHz, our model is again unable to describe the experimental magnitude and phase.

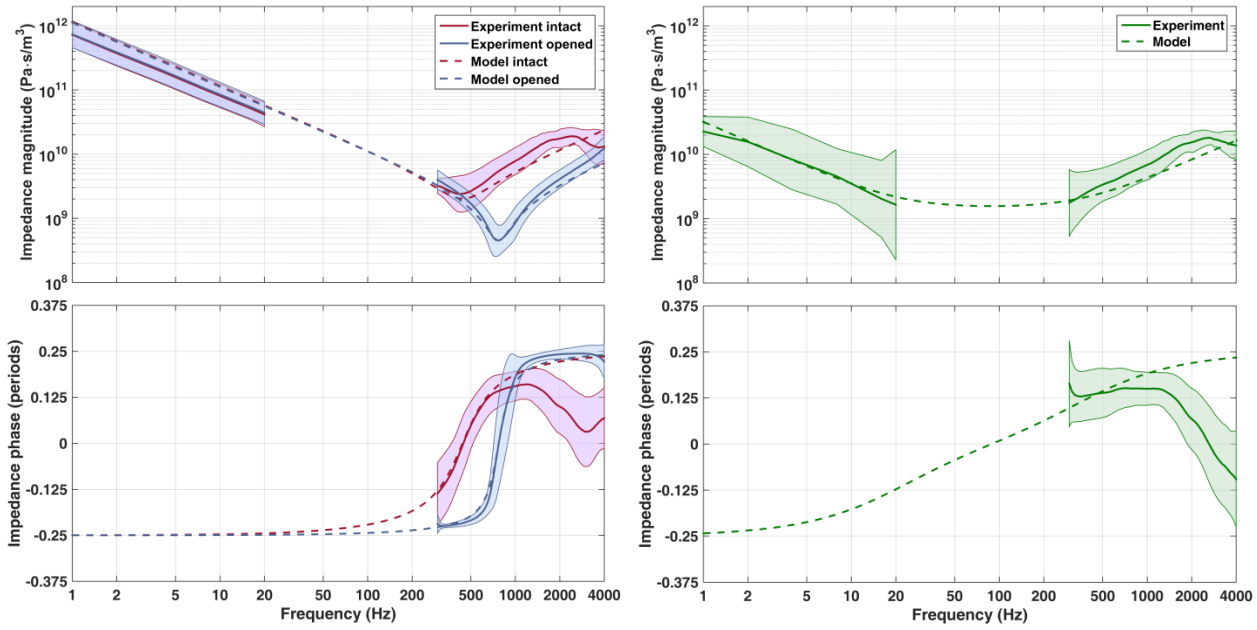

Figure 5. Acoustic impedance magnitude (top) and phase (bottom) for (a) intact and opened IE, and (b) the IE itself as a function of frequency. Full lines represent the mean of the measurements at each frequency for intact IE (red), opened IE (blue) and IE impedance (green), with standard deviations plotted as colored bands. The corresponding RLC models are shown as dashed lines. (For interpretation of the references to colour in this figure legend, the reader is referred to the web version of this article.)

4. Discussion

4.1 Experimental approach

The acoustic input impedance of the IE was determined using the approach of Merchant *et al*. (1996), which was based on measurements of the combined impedance of the stapes, oval window and IE. In other studies (e.g. Aibara *et al*., 2001), the IE impedance was assessed by measuring the pressure in the scala vestibuli directly using a hydrophone or another type of pressure sensor inserted in the IE. However, in our approach the IE was left intact during measurement as opposed to other techniques. Also, we can measure perpendicularly to the FP, which is not possible with the other approaches for which an angle correction is required. In the experiments, only the piston-like component of the columellar vibrations was considered, since it was shown that it is the primary contributor to the pressure in the IE (Decraemer *et al*., 2007).

4.1.1 Sample preparation

Ravicz *et al*. (2000) studied the effect of freezing and thawing on the cochlear input impedance in human temporal bones. They found that air bubbles can penetrate the IE after freezing and thawing of the fresh specimen. This event could reduce the magnitude of the IE impedance, compared to the measurements before freezing. However, when the IE was refilled with saline to remove the air bubbles, IE impedances were restored to the measurements observed in the fresh state. Therefore, we carefully checked each specimen for the presence of air bubbles behind the round window membrane before measurement, using only these samples for which this was not the case. Nevertheless, air bubbles may have been present that were not observed, so our results should be taken with some caution.

Measurements of middle ear input immittance in human temporal bones were demonstrated to be similar to measurements in live ears (Rosowski *et al*., 1990). Also, no significant differences were found in that study between fresh bones and bones that were frozen and thawed. In literature, there are no studies available comparing IE input impedance measurements of live and dead specimens. It is known however (e.g. Kohllöffel, 1972) that death results in an increased mobility of the basilar membrane, which according to Merchant *et al*. (1996) might decrease the IE impedance magnitude by a factor 2 under certain assumptions (Zwislocki, 1975). These findings were described for the human ear and may also apply to the ostrich.

4.1.2 Experiments in the acoustic regime

To determine the vibration velocity of the columella, the assumption was made that columellar FP vibrations are piston-like. From the full-field holography measurements with IE opened between 0.05 and 12.8 kHz it was found that this assumption is not consistently valid with electromagnetic stimulation of the columella: below frequencies of 0.3 kHz, the full-field displacement map of the FP contains two maxima that move out of phase, indicating the presence of a vibrational mode going along with rocking motions of the FP. Apparently, small asymmetries in the geometry of the columella or the placement of the magnet and coil may cause the ossicle to vibrate asymmetrically in this frequency range. We therefore present impedance measurements in the acoustic frequency range above 0.3 kHz, for which it was found that FP vibrations are mostly piston-like with IE opened. However, small asymmetric vibrations may still be present in the motions of the ossicle with IE intact, but according to Hato *et al*. (2003) and Gummer *et al*. (1989b) the IE only affects FP motions in the high frequency range. Yet, this technique has the advantage that only the OW is stimulated as opposed to the RW.

4.1.3 Experiments in the quasi-static regime

The setup used for the quasi-static measurements is suited to measure frequencies up to 0.02 kHz. From visual observation, it was found that the FP moves as a piston in this frequency range. Since the nature of this measurement method is mechanical instead of optical, the force and piezo transducers are unable to keep up with the imposed oscillations at stimulus frequencies above 0.02 kHz. Also, phase information is missing with this technique. Values of the impedance magnitude in the gap between 0.02 and 0.3 kHz can be predicted from the impedance models, as is shown in Fig. 5 (a), and the quasi-static results deliver the stiffness component of the impedance measurements.

For the piezo stimulation, columellar displacement amplitudes of 50 µm were used, which is about two orders of magnitude above naturally occurring motions in response to acoustic stimulation in the ostrich (Arechvo *et al*.,

2013). Because of the extremely small reaction forces involved, it was not possible to get reliable force measurements with smaller displacements. Using the measurements of sound-induced columellar movements presented by Arechvo *et al*. (2013), we can estimate that a FP motion amplitude of 50 µm corresponds to approximately 128 dB sound pressure level. It has however been shown (e.g. Aerts and Dirckx, 2010; Peacock *et al*., 2015) that even at such high sound pressures the nonlinear response of the ear is still more than 40 dB below the linear response. Also in birds (Saunders, 1985), it was found that the response of the middle ear was linear up to 120 dB SPL, and likely for even higher stimulus levels. Therefore, the measured forces can be linearly normalized so the use of Eq. (1) is justified.

4.2 Experimental results

4.2.1 Acoustic impedance analysis

The RLC models in Fig. 5 that were used to fit the experimental data with intact IE, opened IE and IE impedance slightly overestimate the magnitudes in the quasi-static regime, but underestimate the acoustic-frequency data. We presume that this is due to the limited number of measurement samples in the quasi-static frequency range, resulting in a larger uncertainty. Nevertheless, the models mostly are within the experimental standard deviations. For frequencies above 1-2 kHz, the models fail to describe the experimental impedance for intact IE and the IE itself. The magnitude and phase suddenly drop in this regime, which was also observed in humans (Merchant *et al*., 1996). Apparently, the impedance cannot be described by a purely inertial component in this frequency range.

The components of the model impedance were calculated for intact IE (CIE), opened IE (C) and the IE itself (IE). The component values are $K_{CIE} = 7.25 \cdot 10^{12}$ Pa/m³, $M_{CIE} = 0.952 \cdot 10^{6}$ Pa s²/m³ and $R_{CIE} = 2.02 \cdot 10^{9}$ Pa s/m³ for intact IE, $K_C = 7.05 \cdot 10^{12}$ Pa/m³, $M_C = 0.300 \cdot 10^{6}$ Pa s²/m³ and $R_C = 0.54 \cdot 10^{9}$ Pa s/m³ for opened IE, and $K_{IE} = 0.20 \cdot 10^{12}$ Pa/m³, $M_{IE} = 0.652 \cdot 10^{6}$ Pa s²/m³ and $R_{IE} = 1.57 \cdot 10^{9}$ Pa s/m³ for the IE itself. Presumably, K_{IE} is insignificant since the difference between intact and opened IE was negligible in the stiffness-dominated region of low frequencies. K_C mainly represents the impedance of the annular ligament, while M_C represents the combined inertial impedance of the magnet, the columella and the annular ligament.

The mechanical stiffness k_C of the annular ligament can be calculated from $k_C = K_C \cdot A_{FP}^2$, with A_{FP} the mean surface of motion of the FP, resulting in 64.7 N/m. Similarly, the total mechanical mass m_C with IE opened can be determined, yielding 7.54 mg. The magnet has a mass of 3 mg, so the mass of the ligament and the columella should equal 4.54 mg, corresponding to an inertial impedance of $0.181 \cdot 10^{6}$ Pa s²/m³. Micro-CT scans of the right ear in specimen 8 reveal that the mass of the bony columella equals 1.65 mg for a volume of 0.749 mm³ and density of $2.2 \cdot 10^{3}$ kg/m³ (data not shown). Therefore, 2.89 mg remains, which may be attributed to the annular ligament and hydration of the tissue. For M_{CIE} the contribution of the magnet is also subtracted, yielding $0.833 \cdot 10^{6}$ Pa s²/m³.

For M_{IE} the mechanical mass is found to be $m_{IE} = 16.4$ mg, which is supposed to represent the mass of the fluid in the IE. This time, the mass of the magnet is not subtracted since it was already excluded when subtracting Z_C from Z_{CIE}. The total mass inside the IE was estimated to be 111 mg from 3D scans of an ostrich head (Witmer and Ridgely, 2008), for an IE volume of 111 mm³ and fluid density of 10^3 kg/m³. This value is 6.8 times larger than the measured value, indicating that only a small portion of the fluid in the IE influences motions of the columella. The sound input and exit of the IE via the OW and RW only pass through the perilymphatic spaces of the IE (Manley, 1990) which only comprise a minor fraction of the total IE volume. This partially explains the difference in the measured and estimated values of the inertial component of the IE impedance.

4.2.2 Comparison with measurements in mammals

The acoustic input impedance of the IE was studied previously in mammals, based on theoretical considerations (e.g. Zwislocki, 1962, 1965, 1975; Kringlebotn, 1988; Puria and Allen, 1991) and direct and indirect experimental data. These experiments include measurements on human (Merchant *et al*., 1996; Puria *et al*., 1997; Aibara *et al*., 2001; Puria, 2003; Nakajima *et al*. 2009), guinea pig (Dancer and Franke, 1980), cat (Lynch *et al*., 1982), chinchilla (Ruggero *et al*., 1990; Songer and Rosowski, 2007; Slama *et al*., 2010) and gerbil (Overstreet and Ruggero, 2002; Decraemer *et al*., 2007; de La Rochefoucauld *et al*., 2008). Measurements in the ostrich in this study show that the ostrich IE impedance is much smaller than what is found in each of these mammals. The magnitudes found in this study are in the order of 10^{9}-10^{10} Pa s/m³, while in mammals the impedances were found to be one to two orders higher (de La Rochefoucauld *et al*., 2008). In Merchant *et al*. (1996), the impedance components of the human

cochlea were found to be $K_{CIE} = 326 \cdot 10^{12}$ Pa/m³ and $R_{CIE} = 72 \cdot 10^{9}$ Pa s/m³ for intact IE (C = stapes and IE = cochlea in that study; M_{CIE} was not considered), and $K_C = 219 \cdot 10^{12}$ Pa/m³, $R_C = 5.7 \cdot 10^{9}$ Pa s/m³ and $M_C = 543 \cdot 10^{6}$ Pa s²/m³ for drained IE. When comparing each individual component of the measurements in human to our results, it can be concluded that the components are consistently and considerably smaller in the ostrich ear.

At low frequencies, the difference between intact and opened IE is almost negligible, as can be deduced from Fig. 4 (a) and 5 (a). This is different from what is found in mammals (e.g. Merchant *et al*., 1996), in which a small but detectable difference was found between the two conditions. This can be explained by a difference between mammals and birds of the RW to OW area ratio. The RW membrane is assumed to determine the stiffness reactance of the IE, but because in birds it has a much larger area than the OW its contribution to the IE impedance is negligible.

4.2.3 Comparison with measurements in birds

So far, the static and dynamic motions of the avian middle ear have been measured in only few species, using various techniques. The first study was performed by Gaudin (1968) who photographed vibrations of the columella using unspecified positive and negative pressures applied at the TM and observed rotational motions. Saunders and Johnstone (1972) measured the acoustic response of the TM and FP in the Barbary dove using Mössbauer spectroscopy, while Saunders (1985) used a capacitive probe to compare the acoustic response at the TM of the chicken, pigeon, parakeet, canary and cowbird, and found a good correspondence between the audibility curves of the animals and their TM velocity responses. The latter study also reported quantitative information of ME anatomy of these species based on electron microscopy.

Gummer *et al*. (1989a) measured TM and FP responses in the pigeon with the Mössbauer technique to determine the transformer ratio of the ME. In their companion paper (Gummer *et al*., 1989b) the FP response was measured with intact IE, fenestrated IE and drained IE. With intact IE, they observed sharp or broadly tuned anti-resonances in the FP response at higher frequencies that exhibited positive slopes in the velocity phase. This behavior was assigned to the presence of a reflected wave in the IE that originates from motions of internal structures such as the basilar membrane. This wave would introduce an additional vibrational mode that interferes with the presumed piston-like vibrations of the FP. Also in our study, certain samples in Fig. 2 (a) contain broad peaks in the magnitude of the impedance above 2 kHz (i.e. local minima in the velocity magnitude) with negative impedance phase slopes (i.e. positive velocity phase slopes) that are only observed with IE intact. This observation might indicate the presence of a similar mechanism in the ostrich IE.

The quasi-static motions of the ME were studied in the gull, pigeon, gannet and pheasant (Mills and Zhang, 2006; Mills *et al*. 2007). In these species, it was found that large static pressures at the TM are converted into a rocking displacement at the FP to avoid excessive piston-like displacements into the vestibule, thus serving as a protective mechanism. In the ostrich, the quasi-static and dynamic motions of the FP under acoustic stimulation of the TM were measured by Arechvo *et al*. (2013) with LDV. In acoustic frequency range, they found peak displacements between 0.4 and 0.5 kHz with IE intact, which is similar to our findings with magnetic stimulation of the columella. Furthermore, LDV was used to measure the internal coupling of MEs in starlings (Klump and Larsen, 1992), quails (Larsen and Popov, 1995), budgerigars (Larsen *et al*., 2006) and owls (Kettler *et al*., 2016) in the framework of directional hearing.

In future, the knowledge of the IE impedance in the ostrich that was acquired with this study will be used in finite element analyses to examine the influence of the IE on columellar vibrations under acoustic stimulation of the TM. So far, the mechanical properties of the avian ME have only been studied with a rigid rod model of the swiftlet ear (Thomassen *et al*., 2007) and with a finite element model of the duck ME that was validated with vibration measurements (Muyshondt *et al*., 2015). Nevertheless, both studies did not include experimental information of the acoustic IE impedance. On the other hand, the quantitative information of the IE impedance that was obtained will be utilized to investigate sound power flow through the TM and the ME structures.

4.2.4 Scaling to smaller bird species

Generally, the acoustic input impedance of the IE is inversely related to the size of the IE. This is observed when comparing measurements of the cochlear input impedance in human to smaller mammals (de La Rochefoucauld *et al*., 2008). Theoretically, this observation can be explained by dividing the acoustic impedance into three components: stiffness, resistance and mass. The (mechanical) mass *m* of an object is proportional to volume, or the

one-dimensional size x to the power three ($m \sim x^3$). The relation between the mechanical impedance z and the acoustic impedance Z and is $z = Z \cdot A^2$, with A the surface area of the footplate. If we assume that A scales together with the size of the IE, we obtain for the acoustic mass M that $M \sim 1/x$. Thus, the mass component of the acoustic impedance is inversely proportional to IE size. Similarly, for the stiffness component K we can estimate that $K \sim 1/x^3$ and for the resistive component R that $R \sim 1/x^2$ under certain assumptions (Lynch *et al*., 1982). Therefore, the acoustic IE impedance is presumably larger in smaller birds. For instance, the Muscovy duck has an IE volume of 38 mm³ and a footplate surface area of 1.62 mm². For chickens, the IE volume is 32 mm³ and the footplate surface area is 18.2 mm² (obtained from micro-CT data). Using these geometric relations, we can estimate that the mass component of the acoustic IE impedance in ducks would be 1.2 times larger than in the ostrich, while in chickens it would be 1.3 times larger. By extrapolation, one could expect that smaller bird species may also show higher IE impedances than the ostrich.

5. Conclusion

Measurements of the vibrations of the columella allowed us to determine the acoustic input impedance of the IE in the ostrich for frequencies between 1 Hz and 4 kHz. Due to experimental constraints, a gap is present in the data between 0.02 and 0.3 kHz. The mean values of the impedance measurements were fitted by means of a simple RLC model in series, resulting in a stiffness reactance of $K_{IE} = 0.20 \cdot 10^{12}$ Pa/m³, an inertial impedance of $M_{IE} = 0.652 \cdot 10^6$ Pa s²/m³ and a resistance of $R_{IE} = 1.57 \cdot 10^9$ Pa s/m³. These values are one to two orders in magnitude smaller than what is found in mammal ears. Measurements of the acoustic IE impedance revealed that at low frequencies, the difference of the impedance with intact and opened IE is negligible, showing that the RW does not contribute to the stiffness reactance. At high frequencies, we found that the IE impedance cannot be described by a purely inertial component. The inertial impedance of the IE fluids is found to be smaller than total inertia inside the IE.

Acknowledgments

The research was funded by the Research Foundation of Flanders (FWO), grants No. 11T9316N and G049414N. We want to thank William Deblauwe and Fred Wiese for their technical assistance.

References

Aerts, J.R.M., Dirckx, J.J.J., 2010. Nonlinearity as a function of frequency and sound pressure. Hear. Res. 263 (1-2), 26-32. http://dx.doi.org/10.1016/j.heares.2009.12.022.

Aibara, R., Welsh, J.T., Puria, S., Goode, R.L., 2001. Human middle-ear sound transfer function and cochlear input impedance Hear. Res. 152 (1-2), 100-109. http://dx.doi.org/10.1016/S0378-5955(00)00240-9.

Arechvo, I., Zahnert, T., Bornitz, M., Neudert, M., Lasurashvili, N., Simkunaite-Rizgeliene, R., 2013. The ostrich middle ear for developing an ideal ossicular replacement prosthesis. Eur. Arch. Otorhinolaryngol. 270 (1), 37-44. http://dx.doi.org/10.1007/s00405-011-1907-1.

Cheng, J.T., Aarnisalo, A.A., Harrington, E., del Socorro Hernandez-Montes, M., Furlong, C., Merchant, S.N., Rosowski, J.J., 2010. Motion of the surface of the human tympanic membrane measured with stroboscopic holography. Hear. Res. 263 (1-2), 66-77. http://dx.doi.org/10.1016/j.heares.2009.12.024.

Cheng, J.T., Hamade, M., Merchant, S.N., Rosowski, J.J., 2013. Wave motion on the surface of the human tympanic membrane: holographic measurement and modeling analysis. J. Acoust. Soc. Am. 133 (2), 918-937. http://dx.doi.org/10.1121/1.4773263.

Dancer, A., Franke, R., 1980. Intracochlear sound pressure measurements in guinea pigs. Hear Res. 2 (3-4), 191-205. http://dx.doi.org/10.1016/0378-5955(80)90057-x.

De Greef, D., Soons, J.A.M., Dirckx, J.J.J., 2014. Digital stroboscopic holography setup for deformation measurement at both quasi-static and acoustic frequencies. Int. J. Optomechatroni. 8 (4), 275-291. http://dx.doi.org/10.1080/15599612.2014.942928.

de La Rochefoucauld, O., Decraemer, W.F., Khanna, S.M., Olson, E.S., 2008. Simultaneous measurements of ossicular velocity and intracochlear pressure leading to the cochlear input impedance in gerbil. JARO 9 (2), 161-177. http://dx.doi.org/10.1007/s10162-008-0115-1.

Decraemer, W.F., de La Rochefoucauld, O., Dong, W., Khanna, S.M., Dirckx, J.J.J., Olson, E.S., 2007. Scala vestibuli pressure and three-dimensional stapes velocity measured in direct succession in gerbil. J. Acoust. Soc. Am. 121 (5 Pt 1), 2774–2791. http://dx.doi.org/10.1121/1.2709843.

Gaudin, E.P., 1968. On the middle ear of birds. Acta Otolaryngol. 65 (3), 316-326. http://dx.doi.org/10.3109/00016486809120971.

Gummer, A.W., Smolders, J.W.T., Klinke, R., 1989a. Mechanics of a single-ossicle ear: I. The extra-stapedius of the pigeon. Hear. Res. 39 (1-2), 1-14. http://dx.doi.org/10.1016/0378-5955(89)90077-4.

Gummer, A.W., Smolders, J.W.T., Klinke, R., 1989. Mechanics of a single-ossicle ear. II. The columella footplate of the pigeon. Hear. Res. 39 (1-2), 15-26. http://dx.doi.org/10.1016/0378-5955(89)90078-6.

Hato, N., Stenfelt, S., Goode, R.L., 2003. Three-dimensional stapes footplate motion in human temporal bones. Audiol. Neurotol. 8 (3), 140-152. http://dx.doi.org/10.1159/000069475.

Kettler, L., Christensen-Dalsgaard, J., Larsen, O.N., Wagner, H., 2016. Low frequency eardrum directionality in the barn owl induced by sound transmission through the interaural canal. Biol. Cybern. http://dx.doi.org/10.1007/s00422-016-0689-3.

Khaleghi, M., Lu, W., Dobrev, I., Cheng, J.T., Furlong, C., Rosowski, J.J., 2013. Digital holographic measurements of shape and three-dimensional sound-induced displacements of tympanic membrane. Opt. Eng. 52 (10), 101916. http://dx.doi.org/10.1117/1.OE.52.10.101916.

Klump, G.M., Larsen, O.N., 1992. Azimuthal sound localization in the European starling (Sturnus vulgaris): I. physical binaural cues. J. Comp. Physiol. A 170 (2), 243-251. http://dx.doi.org/10.1007/BF00196906.

Kohllöffel, L., 1972. A study of basilar membrane vibrations. III. The basilar membrane frequency response curve in the living guinea pig. Acustica 27 (2), 82-89.

Kringlebotn, M., 1988. Network model for the human middle ear. Scand. Audiol. 17 (2), 75-85. http://dx.doi.org/10.3109/01050398809070695.

Larsen, O.N., Popov, A.V., 1995. The interaural canal does enhance directional hearing in quail (Aves; Coturnix Coturnix japonica). In: Burrows, M., Matheson, T., Newland, P.L., Schupe, H. (Ed.), Nervous Systems and Behaviour. Proceedings of the 4th International Congress of Neuroethology. Georg Thieme Verlag, New York, 313.

Larsen, O.N., Dooling, R.J., Michelsen, A., 2006. The role of pressure difference reception in the directional hearing of budgerigars (Melopsittacus undulatus). J. Comp. Physiol. A 192 (10), 1063-1072. http://dx.doi.org/10.1007/s00359-006-0138-1.

Lynch, T.J., 3rd, Nedzelnitsky, V., Peake, W.T., 1982. Input impedance of the cochlea in cat. J. Acoust. Soc. Am. 72 (1), 108-130. http://dx.doi.org/10.1121/1.387995.

Manley, G.A., 1972. The middle ear of the tokay gecko. J. Comp. Physiol. 8l (3), 239-250. http://dx.doi.org/10.1007/BF00693629.

Manley, G.A., 1990. Peripheral Hearing Mechanisms in Reptiles and Birds. Springer-Verlag, New York. http://dx.doi.org/10.1007/978-3-642-83615-2.

Manley, G.A., Köppl, C., Yates, G.K., 1997. Activity of primary auditory neurons in the cochlear ganglion of the emu Dromaius novaehollandiae: spontaneous discharge, frequency tuning, and phase locking. J. Acoust. Soc. Am. 101 (3), 1560-1573. http://dx.doi.org/10.1121/1.418273.

Merchant, S.N., Ravicz, M.E., Rosowski, J.J., 1996. Acoustic input impedance of the stapes and cochlea in human temporal bones. Hear. Res. 97 (1-2), 30-45. http://dx.doi.org/10.1016/S0378-5955(96)80005-0.

Mills, R., Zhang, J., 2006. Applied comparative physiology of the avian middle ear: the effect of static pressure changes in columellar ears. J. Laryngol. Otol. 120 (12), 1005-1007. http://dx.doi.org/10.1017/S0022215106002581.

Mills, R., Zadrozniak, M., Jie, Z., 2007. Ossicular motion during changes in static pressure in the avian middle ear. In: Huber, A., Eiber, A. (Ed.), Middle Ear Mechanics in Research and Otology. Proceedings of the 4th International Symposium. World Scientific Publishing, Singapore, 21–25. http://dx.doi.org/10.1142/9789812708694_0003.

Muyshondt, P.G.G., Soons, J.A.M., De Greef, D., Pires, F., Aerts, P., Dirckx, J.J.J., 2015. A single-ossicle ear: acoustic response and mechanical properties measured in duck. Hear. Res. http://dx.doi.org/10.1016/j.heares.2015.12.020.

Nakajima, H.H., Dong, W., Olson, E.S., Merchant, S.N., Ravicz, M.E., Rosowski, J.J., 2009. Differential intracochlear sound pressure measurements in normal human temporal bones. JARO 10 (1), 23-36. http://dx.doi.org/10.1007/s10162-008-0150-y.

Norberg, R., 1978. Skull asymmetry, ear structure and function, and auditory localization in Tengmalm's owl, Aegolius funereus (Linne). Phil. Trans. R. Soc. Lond. B 282 (991), 325-410. http://dx.doi.org/10.1098/rstb.1978.0014.

Overstreet, E.H., 3rd, Ruggero, M.A., 2002. Development of wide-band middle ear transmission in the Mongolian gerbil. J. Acoust. Soc. Am. 111 (1 Pt 1), 261–270. http://dx.doi.org/10.1121/1.1420382.

Peacock, J., von Unge, M., Dirckx, J., 2013. Measurement of the vibration of the middle ear ossicles with removed eardrum: A method for quantification of ossicular fixation. Med. Eng. Phys. 35 (1), 1786-1792. http://dx.doi.org/10.1016/j.medengphy.2013.07.012.

Peacock, J., Pintelon, R., Dirckx, J., 2015. Nonlinear vibration response measured at umbo and stapes in the rabbit middle ear. JARO 16 (5), 569-580. http://dx.doi.org/10.1007/s10162-015-0535-7.

Puria, S., Allen, J.B., 1991. A parametric study of cochlear input impedance. J. Acoust. Soc. Am. 89 (1), 287–309. http://dx.doi.org/10.1121/1.400675.

Puria, S., Peake, W.T., Rosowski, J.J., 1997. Sound-pressure measurements in the cochlea vestibule of human cadaver ears. J. Acoust. Soc. Am. 101 (5 Pt 1), 2754-2770. http://dx.doi.org/10.1121/1.418563.

Puria, S., 2003. Measurements of human middle ear forward and reverse acoustics: Implications for otoacoustic emissions. J. Acoust. Soc. Am. 113 (5), 2773–2789. http://dx.doi.org/10.1121/1.1564018.

Ravicz, M.E., Merchant, S.N., Rosowski, J.J., 2000. Effect of freezing and thawing on stapes-cochlear input impedance in human temporal bones. Hear. Res. 150 (1-2), 215-224. http://dx.doi.org/10.1016/S0378-5955(00)00200-8.

Rosowski, J.J., Davis, P.J., Merchant, S.N., Donahue, K.M., Coltrera, M.D., 1990. Cadaver middle ears as models for living ears: comparisons of middle-ear input immittance. Ann. Otol. Rhinol. Laryngol. 99 (5), 403-412. http://dx.doi.org/10.1177/000348949009900515.

Ruggero, M.A., Rich, N.C., Robles, L., Shivapuja, B.G., 1990. Middle-ear response in the chinchilla and its relationship to mechanics at the base of the cochlea. J. Acoust. Soc. Am. 87 (4), 1612–1629. http://dx.doi.org/10.1121/1.399409.

Saunders, J.C., Johnstone, B.M., 1972. A comparative analysis of middle-ear function in non-mammalian vertebrates. Acta. Otolaryngol. 73 (2-6), 353-361. http://dx.doi.org/10.3109/00016487209138952.

Saunders, J.C., 1985. Auditory structure and function in the bird middle ear: an evaluation by SEM and capacitive probe. Hear. Res. 18 (3), 253–268. http://dx.doi.org/10.1016/0378-5955(85)90042-5.

Slama, M.C.C., Ravicz, M.E., Rosowski, J.J., 2010. Middle ear function and cochlear input impedance in chinchilla. J. Acoust. Soc. Am. 127 (3), 1397-1410. http://dx.doi.org/10.1121/1.3279830.

Songer, J.E., Rosowski, J.J., 2007. Transmission matrix analysis of the chinchilla middle ear. J. Acoust. Soc. Am. 122 (2), 932-942. http://dx.doi.org/10.1121/1.2747157.

Thomassen, H.A., Gea, S., Maas, S., Bout, R.G., Dirckx, J.J.J., Decraemer, W.H., Povel, G.D.E., 2007. Do Swiftlets have an ear for echolocation? The functional morphology of Swiftlet's middle ears. Hear. Res. 225 (1-2), 25-37. http://dx.doi.org/10.1016/j.heares.2006.11.013.

Witmer, L.W., Ridgely, R.C., 2008. The paranasal air sinuses of predatory and armored dinosaurs (Archosauria: Theropoda and Ankylosauria) and their contribution to cephalic structure. The Anatomical Record 291 (11), 1362–1388. http://dx.doi.org/10.1002/ar.20794.

Zwislocki, J., 1962. Analysis of the middle-ear function. I. Input impedance. J. Acoust. Soc. Am. 34 (8 Pt 2), 1514-1523. http://dx.doi.org/10.1121/1.1918382.

Zwislocki, J., 1965. Analysis of some auditory characteristics. In: Luce, R.D., Bush, R.R., Galanter, E. (Ed.), Handbook of Mathematical Physiology. Wiley, New York, 3-46.

Zwislocki, J., 1975. The role of the external and middle ear in sound transmission. In: Tower D.B. (Ed.), The Nervous System, Vol. 3, Human Communication and its Disorders. Raven Press, New York, 45-55.